Fatigue-Crack Growth Behavior in the Superelastic and Shape-Memory Alloy Nitinol

A.L. McKELVEY and R.O. RITCHIE

This article presents a study of fatigue-crack propagation behavior in Nitinol, a 50Ni-50Ti (at. pct) superelastic/shape-memory alloy, with particular emphasis on the effect of the stress-induced martensitic transformation on crack-growth resistance. Specifically, fatigue-crack growth was characterized in stable austenite (at 120 °C), superelastic austenite (at 37 °C), and martensite (at −65 °C and −196 °C). In general, fatigue-crack growth resistance was found to increase with decreasing temperature, such that fatigue thresholds were higher and crack-growth rates slower in martensite compared to stable austenite and superelastic austenite. Of note was the observation that the stress-induced transformation of the superelastic austenite structure, which occurs readily at 37 °C during uniaxial tensile testing, could be suppressed during fatigue-crack propagation by the tensile hydrostatic stress state ahead of a crack tip in plane strain; this effect, however, was not seen in thinner specimens, where the constraint was relaxed due to prevailing plane-stress conditions.

I. INTRODUCTION

NITINOL is a thermoelastic alloy with a composition of approximately 50 at. pct Ni and 50 at. pct Ti, which is capable of two successive athermal martensitic phase transformations on cooling from its higher temperature austenite (*B2-CsCl* crystal structure) phase. The first of these is observed below ~25 °C and results in the "R phase" (rhombohedral crystal structure); the second occurs typically below ~0 °C and results in a monoclinic structure, often with a fine lath morphology. These transformations provide Nitinol with its shape-memory behavior, which results from a unique set of material properties, including thermoelasticity,* a low driving force to nucleate a second phase, and a prominent role of twin deformation. In addition, Nitinol can exhibit superelasticity, with recoverable "elastic" strains up to ~8 pct, at temperatures slightly above the austenite finish temperature, A_f; this effect is attributed to a stress-induced reversible martensitic transformation.

*Thermoelasticity is a property of a material that undergoes a martensitic transformation where the laths, which grow continuously on cooling, revert along the same crystallographic path when the alloy is heated.

Because of its shape-memory properties, Nitinol has been used for such applications as pipe couplings and actuators. Its superelastic properties, on the other hand, are used in eyeglass frames, mobile phone antennas, dental braces, and most recently in the biotechnology industry, principally for endovascular stents. All these applications involve repetitive loading, yet surprisingly little information exists on the fatigue-crack growth properties of Nitinol; indeed, to our knowledge, the literature contains only three previous studies.[1,2,3] Moreover, none of these studies provide a systematic examination on the role of temperature, microstructure, and constitutive behavior on crack-growth rates in NiTi.*

*Dauskardt *et al.*[3] did attempt to study the effect of constitutive behavior on rates of fatigue-crack propagation; however, this was achieved by comparing the properties of alloys with different compositions, rather than in the same material.

Accordingly, the focus of this work is to evaluate the effects of temperature, microstructure, and the presence of the reversible stress-induced martensitic phase transformation on the growth of fatigue cracks in a biotechnology Nitinol alloy, specifically by comparing behavior in the stable austenite, superelastic austenite, and martensite structures.

II. EXPERIMENTAL PROCEDURES

A. *Material*

The Nitinol alloy, which was received as 41.3-mm-diameter rod with a composition of 50Ni-50Ti at. pct (55Ni-45Ti wt pct), was heat treated in air at 500 °C for 35 minutes and then ice water quenched to induce an A_f slightly less than 37 °C (so that the alloy would be superelastic at physiological temperatures). X-ray diffractometry and transmission electron microscopy (TEM) were used to confirm that the alloy was fully austenitic (*B2*) after heat treatment. The microstructure was characterized by an inhomogeneous distribution in grain sizes, with clusters of both small and large grains (Figure 1).

Martensite/austenite transformation temperatures were characterized using differential scanning calorimetry (DSC) in an argon atmosphere. Samples (~50 mg) were held at 100 °C until they reached thermal equilibrium, and then were cooled at 10 °C/min to −150 °C; the same scan rate was used on heating as the sample temperature was returned to 100 °C.

B. *Mechanical Testing*

Round-bar uniaxial tensile samples (25.4-mm gage length, 6.4-mm diameter) were used to assess the monotonic constitutive behavior at temperatures between −196 °C and 120

A.L. McKELVEY, formerly Graduate Student, Department of Materials Science and Mineral Engineering, University of California, is Research Scientist, Materials Science Department, Ford Research Laboratory, Dearborn, MI 48121-2053. R.O. RITCHIE, Professor, is with the Department of Materials Science and Engineering, University of California, Berkeley, CA 94720-1760.

Manuscript submitted April 27, 2000.

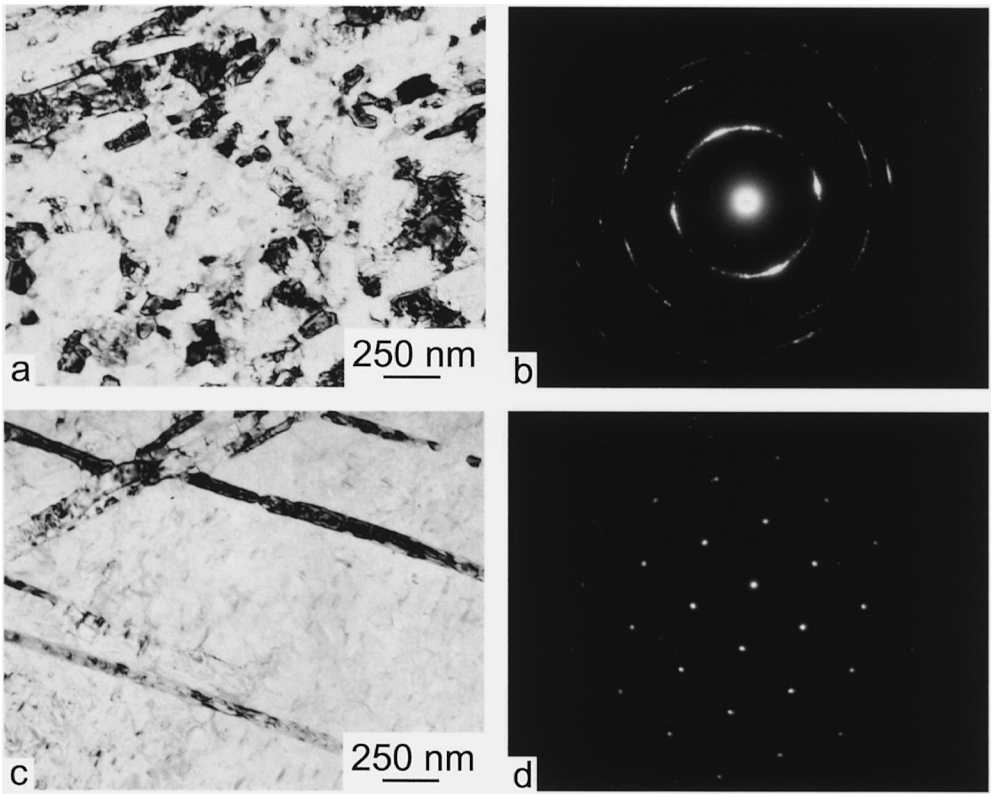

Fig. 1—(*a*) through (*d*) Bright-field transmission electron microscopy images and the respective selected-area diffraction patterns, obtained for Nitinol *in situ* at 37 °C. The microstructure does not show a homogeneous distribution in grain size; instead, there are clusters of small grains, as shown in (a) and (b), and also regions with large grains, seen in (c) and (d).

°C (77 to 393 K). Tests were conducted under displacement control at a strain rate of $\sim 2.67 \times 10^{-5}$ /s (computed from a displacement rate of 2.5 μm/s over the gage length). In some cases, in addition to an axial extensometer, a diametral gage was applied to measure strain through the thickness of the tensile bar.

Fatigue-crack propagation tests were performed on electro-servo-hydraulic testing machines, also between −196 °C and 120 °C. The purpose of varying the temperature was to produce the different structures in Nitinol, namely, stable austenite at 120 °C, superelastic austenite at 37 °C, and martensite at −65 °C and −196 °C. Temperatures were maintained by a variety of techniques: (a) above room temperature, samples were heated in air with infrared heat lamps or in a deionized water bath heated with a TEFLON* coated heating element; (b) below room temperature, they were cooled by either chilled nitrogen gas (−65 °C) or submersed in liquid nitrogen (−196 °C). Temperatures were monitored using a surface resistive-temperature device, to within ±0.2 °C in warm environments and ±1.0 °C at −65 °C; the testing temperature in liquid nitrogen was assumed to be constant.

*TEFLON is a trademark of E.I. DuPont de Nemours & Co., Inc., Wilmington, DE.

Fatigue cycling was carried out at 10 Hz (sine wave) under automated stress-intensity (K) control, with 9-mm-thick disk-shaped compact-tension DC(T) specimens, in general accordance with the procedures described in ASTM standard E647. With this thickness of specimen, plane-strain conditions prevailed for stress intensities at least up to ~60 MPa$\sqrt{\text{m}}$. Crack-propagation rates were measured at constant load ratios (ratio of minimum to maximum loads) of R = 0.1, 0.5, and 0.7. Load shedding schemes with a K gradient (the relative change in stress intensity per unit crack extension) ranging from −0.20 to −0.08 mm^{-1} were used to approach the fatigue threshold, ΔK_{TH}, which was defined as the ΔK value at which growth rates did not exceed $\sim 10^{-10}$ m/cycle. Crack lengths were continuously monitored during cyclic loading using compliance-based methods. In addition, the magnitude of crack closure[4] was estimated in terms of the closure stress intensity, K_{cl}, which was measured as the load corresponding to the first deviation from linearity with respect to displacement on unloading.[5]

Growth-rate (da/dN) data are presented in terms of the applied stress-intensity range, $\Delta K = K_{max} - K_{min}$, where K_{max} and K_{min} are, respectively, the maximum and minimum stress intensities in the fatigue cycle, and the effective (near-tip) stress-intensity range, $\Delta K_{eff} = K_{max} - K_{cl}$, which subtracts out the effect of crack closure.

C. *Characterization*

To aid the understanding of the micromechanisms of damage and crack extension in NiTi during fatigue, TEM studies were performed on electropolished samples taken from within the plastic zone in the crack wake of DC(T) fatigue specimens. To maximize the area fraction of plastic zone in 3-mm-diameter foils, samples were obtained by grinding up to the fatigue surface, such that the large plane of the TEM foils was parallel to the fracture surface. After grinding samples to ~100 μm in thickness, 3-mm discs were mechanically punched followed by electropolishing at −60 °C in

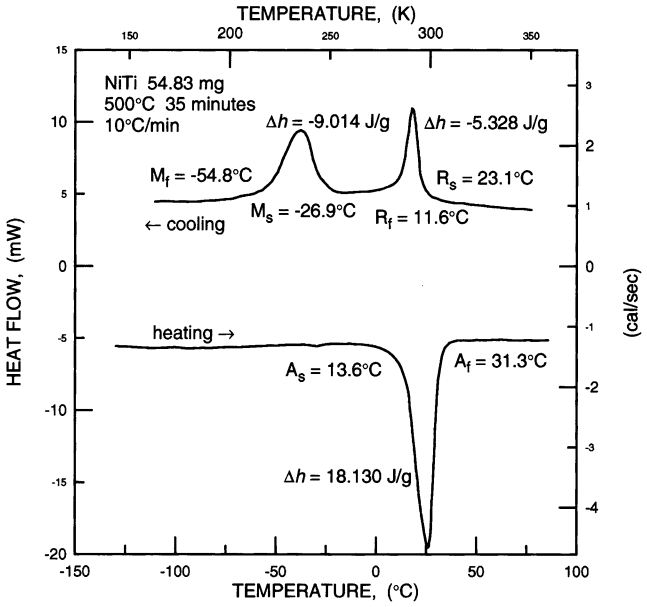

Fig. 2—Differential scanning calorimetry results for NiTi. On cooling, heat was evolved from the sample associated with the transformation from austenite to the rhombohedral phase, often referred to as R phase, which began at 23.1 °C and was complete at 11.6 °C. With further cooling, the martensitic transformation began at −26.9 °C and was finished at −54.8 °C. Upon heating, the temperature ranges for the reverse transformations of the R phase and martensite overlapped, and hence, only one endothermic peak was observed. This peak was associated with the austenite transformation, which started at 13.6 °C and was finished at 31.3 °C.

20 pct HNO_3 and 80 pct methanol at 17 V. Occasionally, it was necessary to view TEM samples *in situ* at the temperature previously applied during fatigue testing; this was to ensure the presence of the same microstructure that existed during the mechanical test.*

*Note that the TEM specimen preparation was independent of the TEM viewing temperature. The TEM foils were electropolished at −60 °C and then allowed to heat to ambient temperature prior to examining by TEM. The microscope was fitted with an *in situ* heating/cooling stage (−196 °C $< T <$ 1000 °C), such that samples could be examined at the same temperature as the fatigue-crack growth temperature. Since the martensite transformation is reversible, material which thermally transformed to martensite during electropolishing, returned to austenite when heated above 31 °C in the *in situ* heating stage of the transmission electron microscope. Further details of TEM specimen preparation for NiTi have been carefully described by Michal.[6]

III. RESULTS AND DISCUSSION

A. *Transformation Temperatures*

Calorimetry revealed the presence of three phase transformations, as shown in Figure 2. On cooling, the transformation from austenite (*B*2) to the rhombohedarl R phase[7] began at ~23.1 °C ($T = R_s$) and was complete at 11.6 °C ($T = R_f$). With further cooling, the martensitic[8] transformation began at −26.9 °C ($T = M_s$) and was finished at −54.8 °C ($T = M_f$). No further phase changes occurred as the temperature was lowered to −150 °C. Upon heating, the temperature ranges for the reverse R phase and martensitic transformations overlapped, and hence, only one endothermic peak was observed,[7,9–11] corresponding to the austenite transformation, which started at 13.6 °C ($T = A_s$) and finished at 31.3 °C ($T = A_f$). The enthalpies for each reaction were −5.328, −9.014, and +18.130 J/g for the R phase, martensite, and austenite transformations, respectively. Over the temperature range A_f to M_d, where M_d is defined as the upper limit for the existence of stress-induced martensite, the material is expected to relieve strain energy when under a critical load by a phase transformation. Data to support the determination of M_d in the present alloy are published elsewhere;[12] the value of M_d was found to be ~80 °C.

B. *Tensile Constitutive Behavior*

1. *Austenite (stable and superelastic)*

To verify that NiTi was superelastic, the lack of permanent residual deformation had to be measured on a sample loaded to greater than 1 pct strain. This test was conducted at 37 °C, on a sample arbitrarily displaced to ~4.5 pct strain and then unloaded (Figure 3(a)). The alloy displayed linear elastic distortion until the critical stress (~407 MPa) for martensite nucleation. The volume fraction of martensite increased along the loading plateau until unloading at ~4.5 pct strain; the stress then decreased to ~200 MPa, at which point the volume fraction of martensite decreased along the lower stress plateau.[13,14] After complete unloading, there was no detectable permanent strain, and hence, the transformation was superelastic and geometrically reversible. The complete uniaxial constitutive behavior at 37 °C is shown in Figure 3(b). The alloy displayed a loading stiffness of 62 GPa up to the critical martensite nucleation stress (~407 MPa); once the martensitic transformation was essentially complete at ~4.7 pct strain, the stress began to increase again with a loading stiffness of 22 GPa (measured with an axial extensometer). The 0.2 pct offset plastic-yield point from the second linear elastic region was 1058 MPa at a strain of 8.2 pct; the strain-to-failure, ε_f, was 21.3 pct (for a 25.4-mm gage length).

At high enough temperatures (*i.e.*, $T > M_d$), the loading plateau associated with the stress-induced martensitic transformation was not observed; instead, the material remained stable as the austenite phase. A plot of this uniaxial constitutive behavior at 120 °C is also shown in Figure 3(b). At this temperature, the material displayed an elastic loading stiffness of 74 GPa, with a 0.2 pct offset plastic-yield strength of 715 MPa. Following yielding, substantial work hardening was observed until the sampled failed at $\varepsilon_f = 11.0$ pct.

2. *Martensite*

As martensite can be formed in the present material at temperatures less than −55 °C (M_f), tensile tests were conducted at −65 °C and at −196 °C (Figure 3(b)). When loaded at −65 °C, martensite laths began to reorient at very low applied stress,[13,14] *i.e.*, less than 50 MPa. This process was complete after approximately 5 pct strain, where the stress response began to converge with the superelastic (37 °C) data with continued loading. At −196 °C (77 K), a similar trend was observed; however, a higher stress (*i.e.*, 300 MPa) was required to initiate lath reorientation.

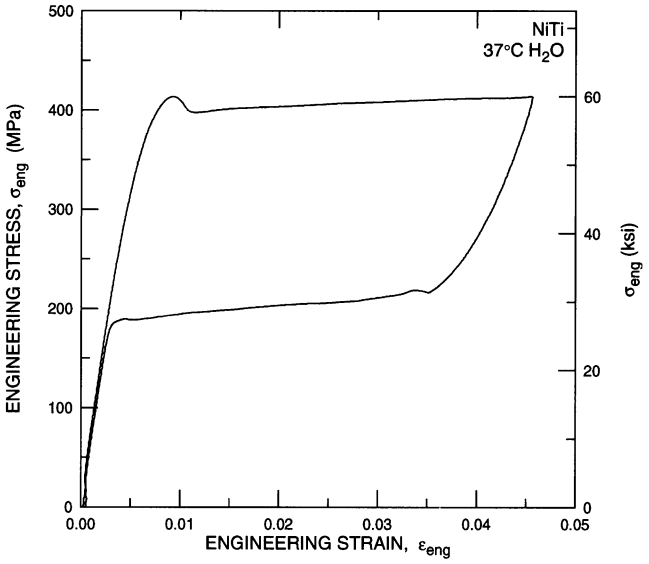

(*a*)

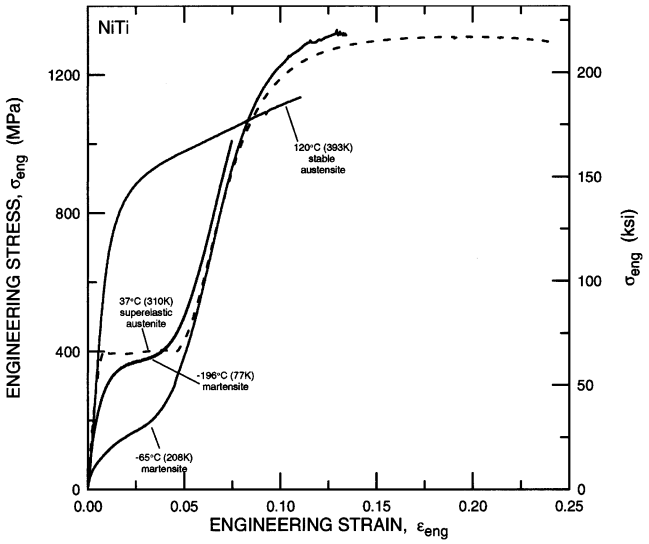

(*b*)

Fig. 3—Uniaxial stress-strain curves for Nitinol showing (*a*) the fully reversible superelastic transformation for superelastic austenite at 37 °C, and (*b*) comparable behavior for stable austenite at 120 °C, and martensite at temperatures of −65 °C and −196 °C. Note in (a) how the superelastic austenite shows linear elastic distortion until the critical stress to nucleate martensite (~407 MPa) is reached; the volume fraction of martensite increases along the loading plateau, before decreasing on unloading below 200 MPa along the lower plateau.

C. *Effect of Constitutive Behavior on Fatigue-Crack Growth*

1. *Stable austenite*

The fatigue-crack growth behavior of stable austenite was characterized at 120 °C, *i.e.*, above M_d (80 °C). This microstructure was considered a "control" material, as no stress-induced phase transformations or lath reorientation processes were possible at this temperature. The effect of varying load ratio ($0.1 \leq R \leq 0.7$) on rates of fatigue-crack propagation as a function of the stress-intensity range, shown in Figure 4(a), indicates that growth rates, *da*/*dN*, are increased (in the mid-growth or Paris regime) by almost an order of magnitude as R is raised from 0.1 to 0.7; corresponding ΔK_{TH} thresholds are decreased from ~2.5 MPa$\sqrt{m}$ at $R = 0.1$ to ~1.5 MPa$\sqrt{m}$ at $R = 0.7$. Such load-ratio-dependent behavior in metallic materials can generally be ascribed to one of two mechanisms, namely, crack closure (which predominates at low ΔK levels) (*e.g.*, Reference 15) or K_{max}-dependent fracture mechanisms (which most often occurs at high ΔK levels approaching instability;[16] these mechanisms often can be distinguished by replotting the growth-rate data in terms of, respectively, ΔK_{eff} and K_{max}. Closure effects only occur up to a critical value of R, above which $K_{min} > K_{cl}$.[15] By replotting the data in Figure 4(a) in terms of ΔK_{eff}, the effect of R can be seen to be significantly reduced at low stress-intensity ranges (Figure 4(b)), indicating that the R dependent behavior at near-threshold levels is largely a function of closure. Closure, however, appears to be less important at higher growth rates as the data are not well scaled at $\Delta K_{eff} > 4$ MPa$\sqrt{m}$. Conversely, where K_{max}-controlled fracture mechanism ("static modes") predominate, the effect of load ratio can generally be normalized by plotting in terms of K_{max};[17] however, this is clearly not apparent for Nitinol (Figure 4(c)).

This aspect can be better appreciated by simply expressing the crack-growth data in terms of a modified Paris power-law relationship, which includes the effect of both ΔK and K_{max} on growth rates:[18]

$$da/dN = C'(K_{max})^n(\Delta K)^p \qquad [1]$$

where C' is a scaling constant (independent of K_{max}, ΔK, and R), and n and p are experimentally determined crack-growth exponents.* A regression fit to the data in Figure 4 yields values of $n = 1.7$ and $p = 1.7$, which clearly illustrates the similar sensitivity of growth rates to ΔK and to K_{max} (Table I). Nitinol, although not very brittle (strain to failure at 37 °C is ~21 pct), is an intermetallic with an ordered *B2* crystal structure, and it is a characteristic of intermetallics to have nominally similar p and n exponents (compared to metals where $p >> n$ and ceramics where $n >> p$ [19]). For example, values of $p \sim 10.3$ and $n \sim 5.6$ have been measured for an XD gamma-based titanium aluminide[20] and $p \sim 7.5$ and $n \sim 13.2$ in a Nb-reinforced molybdenum disilicide composite.[21] The fact that p and n are equal in stable austenitic NiTi is consistent with why the growth-rate data for different load ratios cannot be normalized by characterizing solely in terms of either ΔK_{eff} or K_{max} (unlike metals where ΔK_{eff} provides the optimal normalization, and conversely, in ceramics, where it is K_{max}[19]).

*Equation [1] relates to the usual form of the Paris relationship, $da/dN = C(\Delta K)^n$, by noting that $K_{max} = \Delta K/(1 - R)$, such that $m = n + p$ and $C = C'/(1 - R)^n$.

2. *Superelastic austenite*

Corresponding fatigue-crack propagation results for superelastic austenite at 37 °C (A_f = 31 °C) are shown in Figure 5. Similar to the stable austenite structure, ΔK_{TH} threshold values decreased with increasing R, from ~2.0 MPa$\sqrt{m}$ at $R = 0.1$ to ~1.0 MPa$\sqrt{m}$ at $R = 0.7$, with an accompanying order of magnitude increase in growth rates (in the Paris regime). Characterization in terms of ΔK_{eff} (Figure 5(b)) showed some degree of scaling of the different load ratio data at low growth rates, which once again indicated a prominent role of crack closure at near-threshold

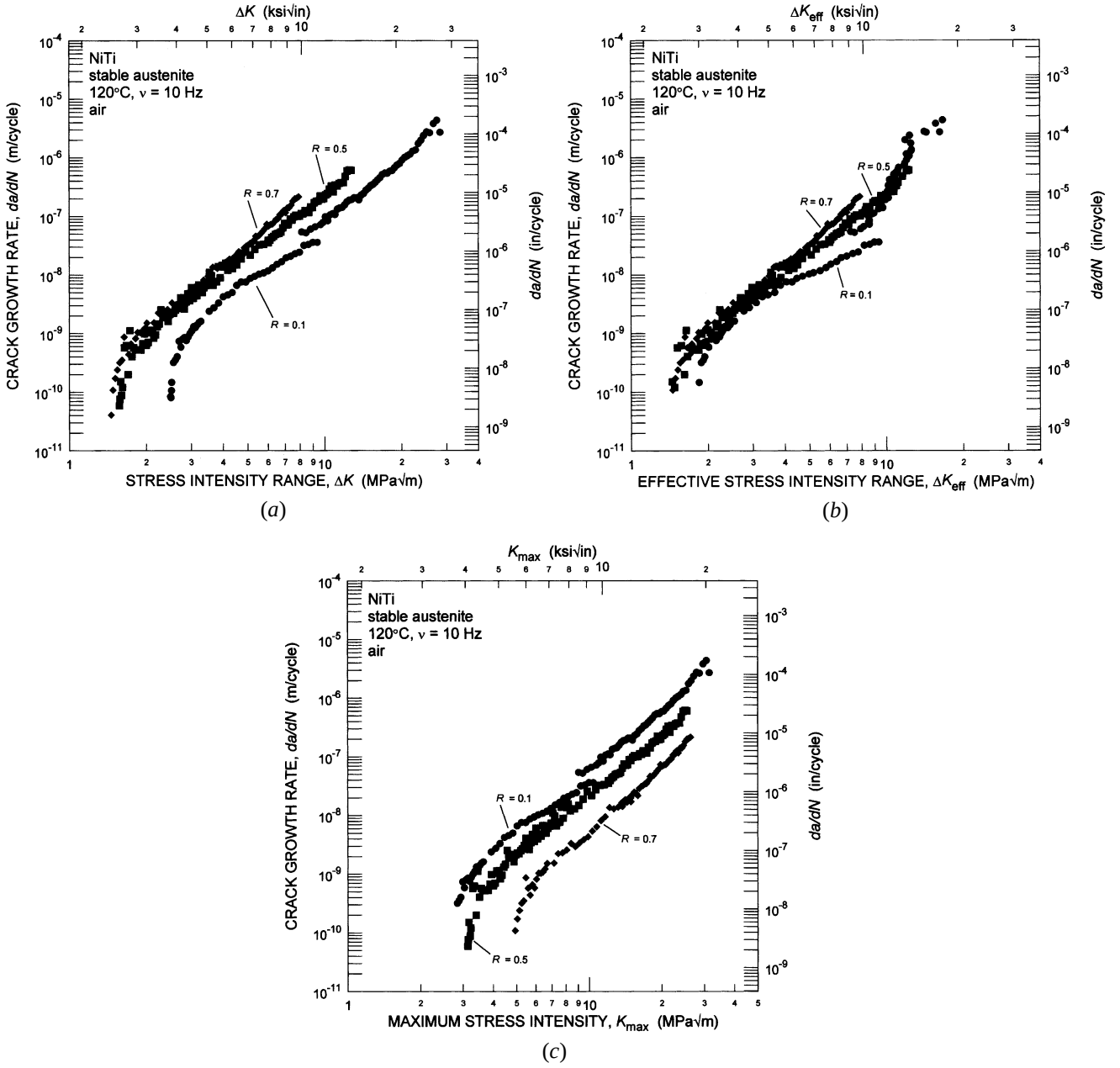

Fig. 4—Rates of fatigue-crack propagation are shown for stable austenitic Nitinol at 120 °C at load ratios of $R = 0.1$, 0.5, and 0.7, as a function of (*a*) the applied ΔK; (*b*) the near-tip ΔK_{eff}, after "correcting" for crack closure; and (*c*) the maximum stress intensity, $K_{\max}$.

Table I. Summary of Modified Paris-Law Parameters

Microstructure	C', m/cycle	p; $(\Delta K)^p$, MPa$\sqrt{\text{m}}$	n; $(K_{\max})^n$, MPa$\sqrt{\text{m}}$
Stable austenite	2.747×10^{-11}	1.7	1.7
Superelastic austenite	3.049×10^{-11}	1.2	2.0

levels; however, as with the stable austenite, plotting in terms of $K_{\max}$ (Figure 5(c)) provided no further normalization.

In terms of the modified Paris power-law formulation (Eq. [1]), the exponents for superelastic austenite, $n = 1.2$, $p = 2$, were again nominally similar indicating a balanced role of alternating and maximum stresses.

Such behavior in transforming superelastic austenite, where the effect of closure is significant only close to ΔK_{TH}, is consistent with behavior in many metallic materials,[22] yet distinct from reported results on another transforming material, 304 stainless steel.[23] Here, the irreversible stress-induced martensitic transformation was claimed to induce

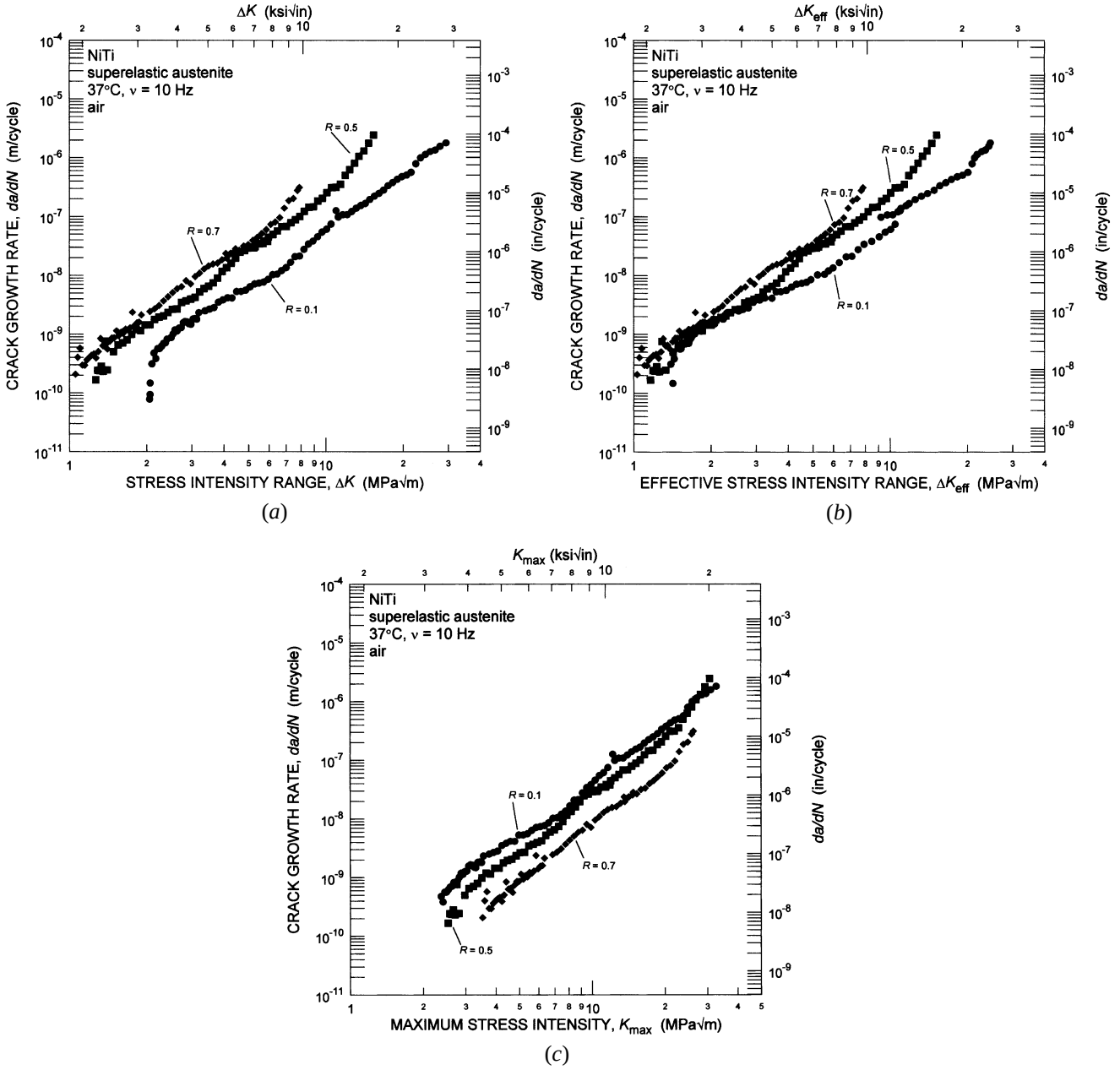

Fig. 5—Rates of fatigue-crack propagation are shown for superelastic austenitic Nitinol at 37 °C at load ratios of $R = 0.1$, 0.5, and 0.7, as a function of (*a*) the applied ΔK; (*b*) the near-tip ΔK_{eff}, after correcting for crack closure; and (*c*) the maximum stress intensity, K_{max}.

sufficient crack-tip shielding such that $K_{cl} > K_{\text{min}}$ at all ΔK levels; the results of this was that ΔK_{eff} scaled the growth rates at different load ratios ($0.05 < R < 0.5$) over the entire range of ΔK from threshold to instability. In contrast, the influence of crack closure in causing load-ratio-dependent behavior is limited to near-threshold stress-intensity ranges (*i.e.*, at $\Delta K_{\text{eff}} < 4.0$ MPa$\sqrt{\text{m}}$) in superelastic Nitinol.

3. *Martensite*

Fatigue-crack propagation results for the martensite structure were obtained at −65 °C and −196 °C at $R = 0.1$ (10 Hz) and are shown in Figure 6. Above $\Delta K \sim 6.5$ MPa$\sqrt{\text{m}}$, growth rates are essentially insensitive to temperature. However, at near-threshold levels, growth rates are reduced at the lower temperature, with a corresponding increase in the ΔK_{TH} threshold from ~3 MPa$\sqrt{\text{m}}$ at −65 °C to ~5 MPa$\sqrt{\text{m}}$ at −196 °C. The trend of increasing ΔK_{TH} thresholds with decreasing temperature is commonly observed in many metallic systems.[24,25]

D. *Comparison of Fatigue Data as a Function of Temperature*

In general, the fatigue-crack growth resistance of Nitinol increases with decreasing temperature (Figure 7). Specifically, there is approximately an order of magnitude decrease in near-threshold growth rates between 37 °C and −65 °C, and an accompanying ~50 pct increase in the threshold, *i.e.*, $\Delta K_{\text{TH}} \sim 2$ MPa$\sqrt{\text{m}}$ for superelastic austenite at 37 °C compared to ~3 MPa$\sqrt{\text{m}}$ for the martensite at −65 °C. Indeed, the fatigue threshold for martensite continues to

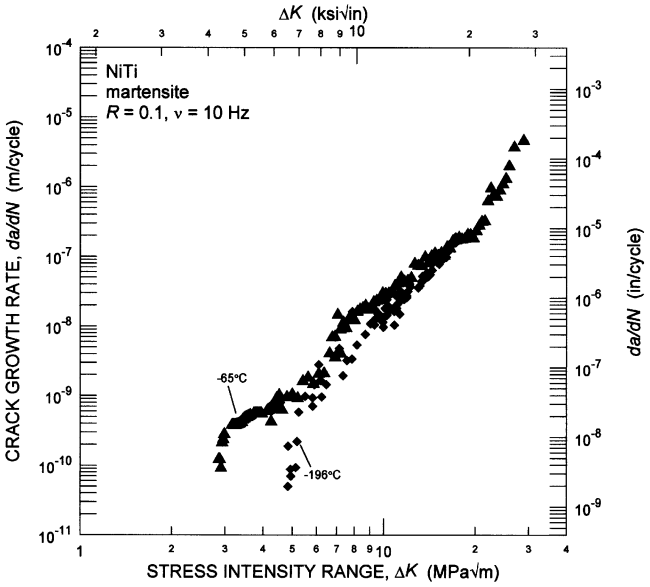

Fig. 6—Rates of fatigue-crack propagation are shown for martensitic Nitinol at −65 °C and −196 °C (77 K) at a load ratio of $R = 0.1$ as a function of the applied ΔK. As temperature decreases, ΔK_{TH} increases from ~3.0 MPa$\sqrt{\text{m}}$ at −65 °C to ~5.0 MPa$\sqrt{\text{m}}$ at −196 °C. At $\Delta K >$ 6.5 MPa$\sqrt{\text{m}}$, the growth-rates converge and are similar.

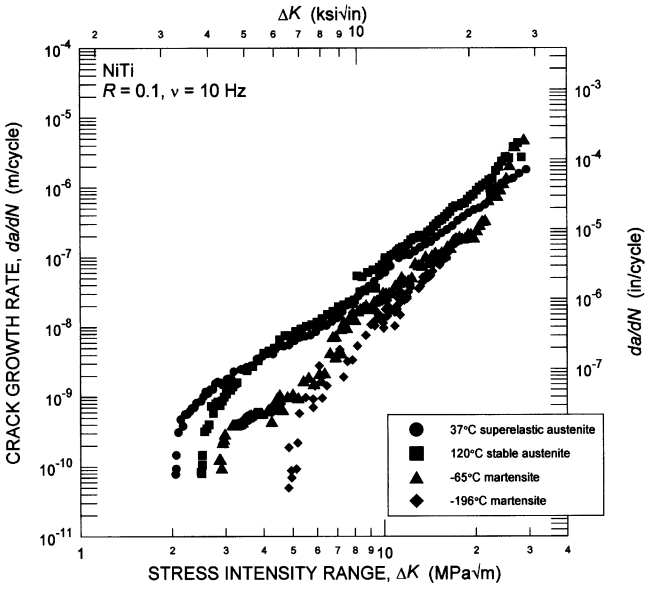

Fig. 7—Comparison of the fatigue-crack growth behavior in Nitinol as a function of temperature, microstructure, and constitutive behavior, showing behavior in stable austenite (120 °C), superelastic austenite (37 °C), and martensite (−65 °C and −196 °C). With the exception of stable austenite at 120 °C, as the temperature decreases, the ΔK_{TH} threshold is increased while the growth rates are decreased.

increase with further reduction in temperature, rising to ~5.0 MPa$\sqrt{\text{m}}$ at −196 °C. Although it is difficult here to separate the individual roles of temperature and microstructure,* particularly since there is no single trend of how the threshold ΔK_{TH} varies with temperature in nontransforming metals,** it is interesting to note that of the Nitinol structures studied, both in the current and previous[3] studies, superelastic austenite has the *worst* fatigue-crack growth properties, yet ironically, it is the most popular microstructure for commercial applications.

Scanning electron micrographs of the fatigue fracture surfaces of the austenitic and martensitic structures at intermediate growth rates (at $\Delta K \sim 10$ MPa$\sqrt{\text{m}}$) are shown in Figure 8; crack-growth behavior in this regime is relatively insensitive to microstructure. The fracture morphologies show no distinct features, although the martensitic structures, which were tested at the lowest temperatures, are more faceted and "brittle-like." Corresponding fatigue fracture surfaces at near-threshold levels (Figure 9), where there is a large effect of microstructure on crack-growth rates, are far smoother in appearance, although the martensitic structures do show somewhat increased roughness. Such surface roughness can enhance fatigue-crack growth resistance by promoting crack closure, particularly near ΔK_{TH}.[22]

E. *Superelastic vs Stable Austenite*

A comparison of fatigue-crack growth rates in superelastic and stable austenite (at 37 °C and 120 °C, respectively) as a function of load ratio (at 10 Hz) is shown in Figure 10. Despite the marked difference in the monotonic constitutive behavior (Figure 3(b)) due to the *in-situ* stress-induced martensitic transformation in the superelastic structure, there is remarkably little difference in the fatigue-crack growth behavior of the two structures at all load ratios, except at near-threshold levels below $\sim 10^{-9}$ m/cycle where the stable austenitic structure displays slightly higher ΔK_{TH} (<1 MPa$\sqrt{\text{m}}$ higher). Since mechanically induced phase transformations have been exploited in the past to promote fracture resistance in several metallic and ceramic materials (*e.g.*, Reference 22), the superelastic transformation in NiTi was believed to be a potential source of toughness and fatigue resistance.[3] The current result, however, is both unexpected and significant as it implies that *superelasticity does not appear to enhance the fatigue-crack growth resistance of Nitinol*.

1. *Influence of plasticity on superelasticity*

To understand this phenomenon, we first examine the effect of plastic strain on superelasticity. When superelastic austenite is loaded to approximately the ultimate tensile strength (UTS), and then unloaded prior to failure (Figure 11), the transformation strain is not recovered and the deformation is permanent (excluding the recoverable linear elastic unloading strain). For the present alloy at 37 °C, the martensitic transformation took place at an applied stress of ~400 MPa and was complete after ~5 pct strain, whereupon a second region of linear elastic distortion occurred until the

*In an attempt to evaluate the relative mechanical properties of stable austenite, superelastic austenite, and martensite in Nitinol, the structures were compared in a previous study[3] *at the same temperature* (22 °C) by adjusting the composition of NiTi, whereas in the current work, the comparison has been made *with the same composition* by varying the temperature. Since alloy composition, microstructure, and temperature all clearly affect the fatigue properties, a perfect "clean" comparison between the various structures in Nitinol is difficult to achieve.

**Based on the concept of critical crack-tip opening displacement at the threshold, with decrease in temperature, the resulting increase in yield strength should lead to an increase in ΔK_{TH} (*e.g.*, Ref 24); however, this simple notion does not uniformly apply as it does not take into account such additional factors as variations in crack closure, fracture mode, and environmental effects.

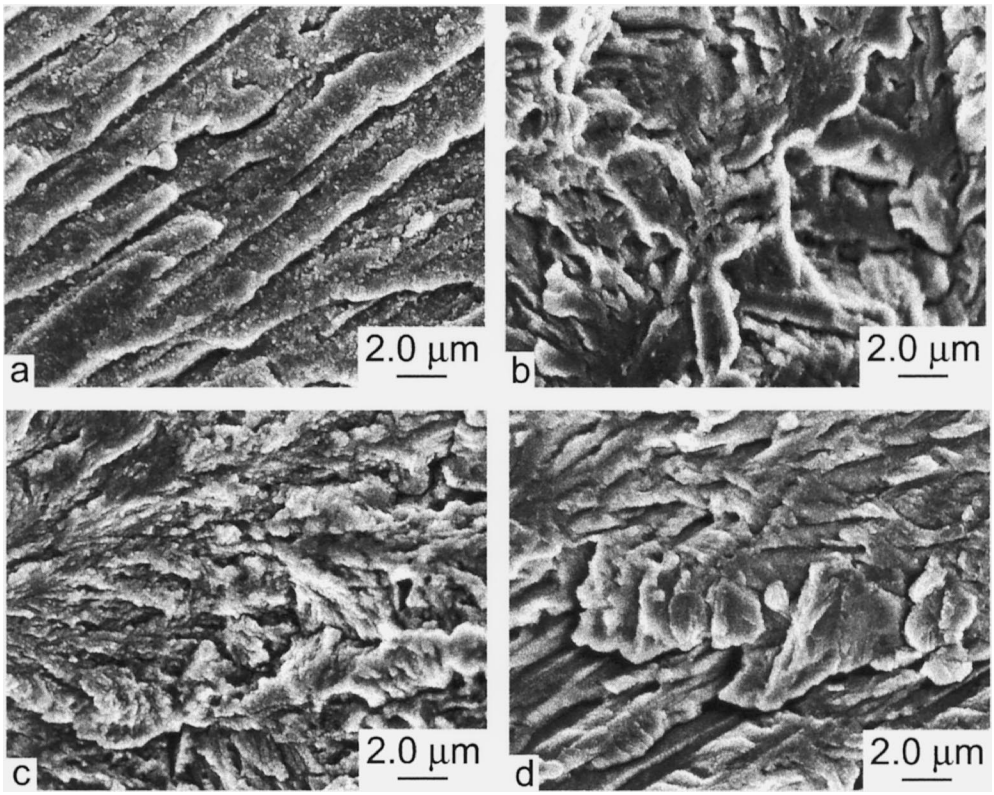

Fig. 8—A comparison of fatigue fracture surfaces at $\Delta K \sim 10$ MPa$\sqrt{\text{m}}$ for (*a*) stable austenite at 120 °C, (*b*) superelastic austenite at 37 °C, (*c*) martensite at −65 °C, and (*d*) martensite at −196 °C. Note that while all surfaces appear rough, there is a transition from a ductile (*e.g.*, stable austenite) to a more brittle (*e.g.*, martensite at −196 °C) failure mode. The direction of crack growth is from left to right.

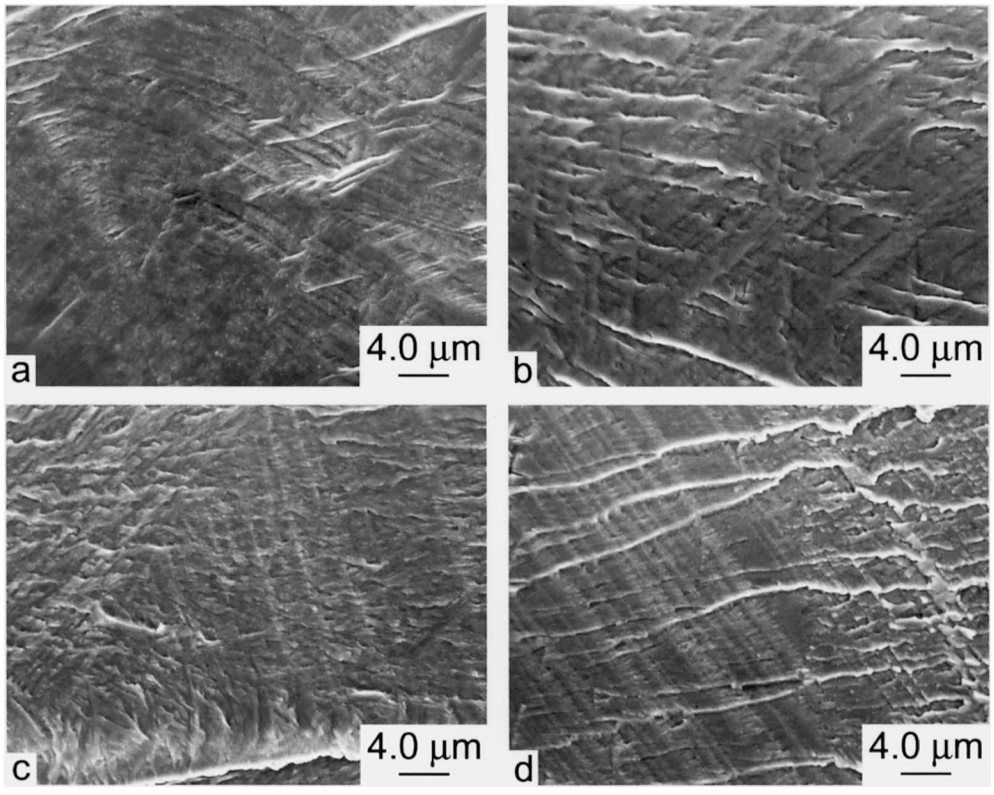

Fig. 9—A comparison of fatigue fracture surfaces near the ΔK_{TH} threshold for (*a*) stable austenite at 120 °C, (*b*) superelastic austenite at 37 °C, (*c*) martensite at −65 °C, and (*d*) martensite at −196 °C. Note that while all surfaces appear smooth compared to fractography at $\Delta K \sim 10$ MPa$\sqrt{\text{m}}$, there is an increase in roughness as the temperature is lowered. The direction of crack growth is from left to right.

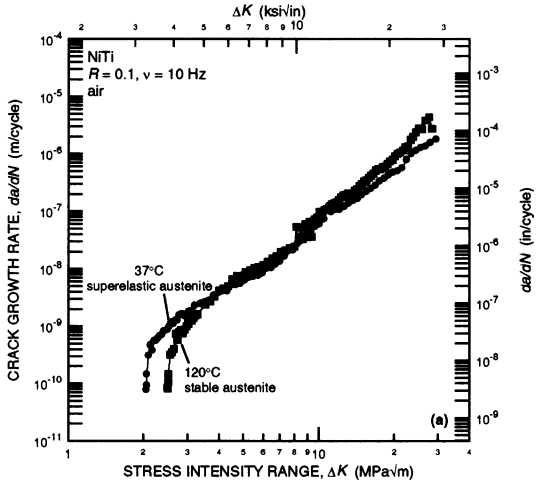

(*a*)

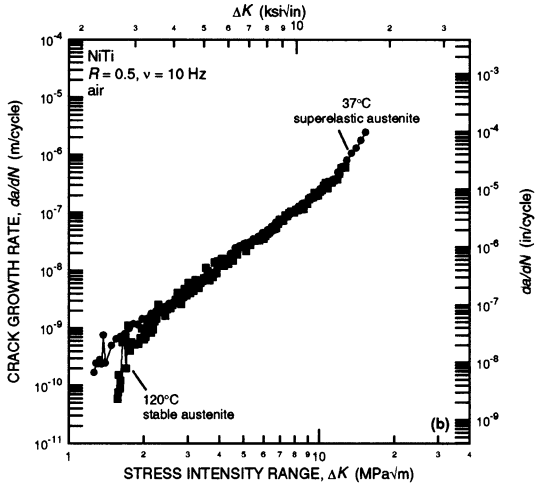

(*b*)

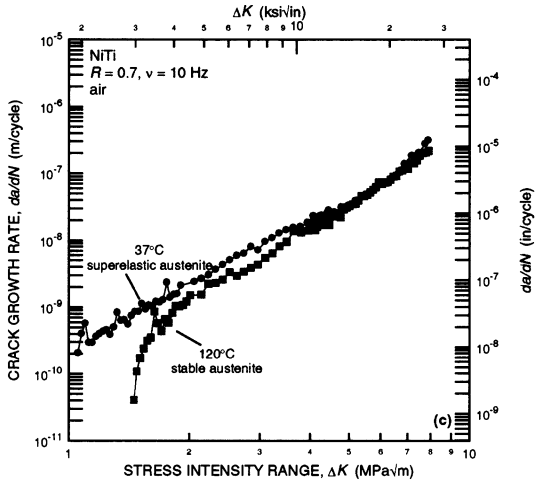

(*c*)

Fig. 10—Comparison of fatigue-crack growth rates as a function of the applied ΔK in stable (120 °C) and superelastic austenite (37 °C) at load ratios of (*a*) 0.1, (*b*) 0.5, and (*c*) 0.7. The data are similar and essentially insensitive to microstructure except for a small difference at near-threshold levels at all load ratios.

plastic yield strength was exceeded at ~1058 MPa. In the present test, the sample was unloaded completely once the

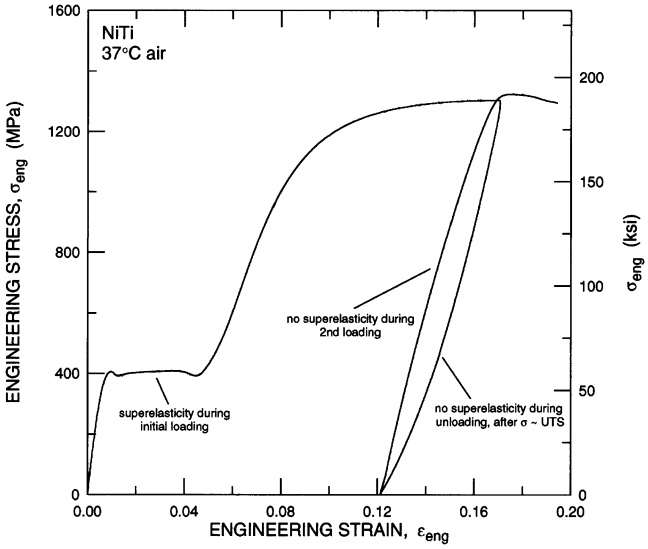

Fig. 11—A plot of tensile test data in superelastic austenite (37 °C), which illustrates that plastic deformation (*i.e.*, $\sigma \sim$ UTS) destroys superelastic recovery.

applied stress reached ~UTS (Figure 11). During the unloading, no superelastic recovery was observed; instead, the permanent strain was ~12 pct; this is in contrast to behavior without plasticity (Figure 3(a)), where a sample displayed complete recovery after unloading from ~4.5 pct axial strain. When the sample was reloaded, no superelastic plateau was observed as the stress was increased to ~UTS, where the material began to deform until final fracture (Figure 11). This experiment indicates that plastic strain can stabilize stress-induced martensite such that the transformation becomes irreversible.

This conclusion was verified by X-ray diffraction studies on sections of the tensile bar after unloading; these showed that the monoclinic martensitic structure had been stabilized at 37 °C and was the predominant phase.*

*Details of this, and other X-ray spectra given in this article, can be found in Ref. 26.

A more complete characterization of this phenomenon of plasticity-degraded superelasticity is shown in Figure 12, again for the monotonic tensile loading of NiTi at 37 °C. Plotted is the normalized recovery strain, $(\varepsilon_{applied} - \varepsilon_{residual})/\varepsilon_{applied}$, as a function of the normalized applied strain, $\varepsilon_{applied}/\varepsilon_{plastic}$, where $\varepsilon_{applied}$, $\varepsilon_{residual}$, and $\varepsilon_{plastic}$ are, respectively, the maximum applied strain prior to unloading, the residual strain after complete unloading, and the value of strain associated with the 0.2 pct offset plastic yield strength in the second linear portion of a superelastic constitutive curve. It can be seen that as the applied strain increases, the magnitude of the normalized recovery strain is decreased, with a significant reduction occurring once the plastic yield strength is exceeded, *i.e.*, when $\varepsilon_{applied}/\varepsilon_{plastic} > 1.0$ at $\varepsilon_{applied} \sim 8.5$ pct. At values of $\varepsilon_{applied}/\varepsilon_{plastic}$ greater than ~1.25, the normalized recovery strain approaches the locus for linear-elastic recovery of a purely martensite polycrystal.

2. *Superelasticity at a crack tip*

Since plastic strain can stabilize the martensite phase, a pertinent question is what may happen ahead of a growing fatigue crack in superelastic austenite at 37 °C. If the material

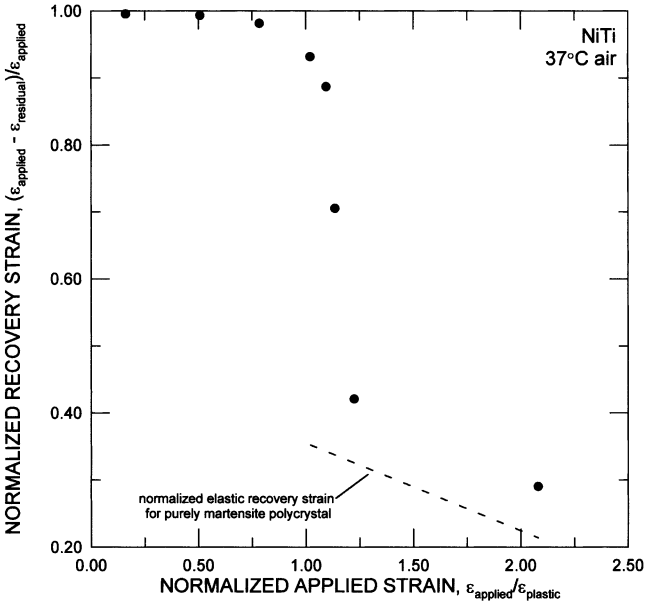

Fig. 12—Results showing how the normalized recovery strain is dramatically reduced when the applied strain, $\varepsilon_{applied}$, exceeds the plastic-yield strain (0.2 pct offset), $\varepsilon_{plastic}$.

near the crack tip were transforming under an applied load, then this zone of stress-induced martensite would experience a high level of deformation. Based on the information shown in Figure 12,* material in the crack wake, and thus eventually on the fatigue fracture surface, should be plasticity-stabilized martensite; moreover, as the transformation occurs ahead of the crack, the crack tip would be growing into the martensite, and not the superelastic austenite, phase. If this hypothesis were true, then the fatigue-crack growth behavior of superelastic austenite and martensite (neglecting temperature effects) should be the same; however, as shown in Figure 7, the data are quite different. The ΔK_{TH} threshold for martensite (at −65 °C) is some 50 pct higher than for superelastic austenite, with near-threshold growth rates being approximately an order of magnitude slower.

*It is appreciated that the tensile results in Fig. 12 pertain to a very different stress state than that existing ahead of a crack tip in plane strain. However, constitutive data for the deformation of superelastic NiTi under triaxial stress states are not available at this time.

These observations strongly suggest that material at the crack tip may not have transformed during fatigue-crack growth in superelastic Nitinol at 37 °C, because (1) crack-growth rates in the stable and superelastic structures are very similar and (2) corresponding growth rates in the superelastic austenite and martensite structures are quite different (Figure 7). To examine this further, transmission electron microscopy was used to image material within the plastic zone of fatigue specimens to determine which phase was present. Bright-field images of this region (Figure 13(a)) display a far higher density of dislocations than in the virgin alloy (Figure 1); moreover, they do not show the characteristic martensite lath structure. Indeed, selected area diffraction of the same region (Figure 13(b)) reveals that the phase is austenite, indicating that the material within the plastic zone in the crack wake had not transformed.

To verify this conclusion, X-ray diffraction was performed

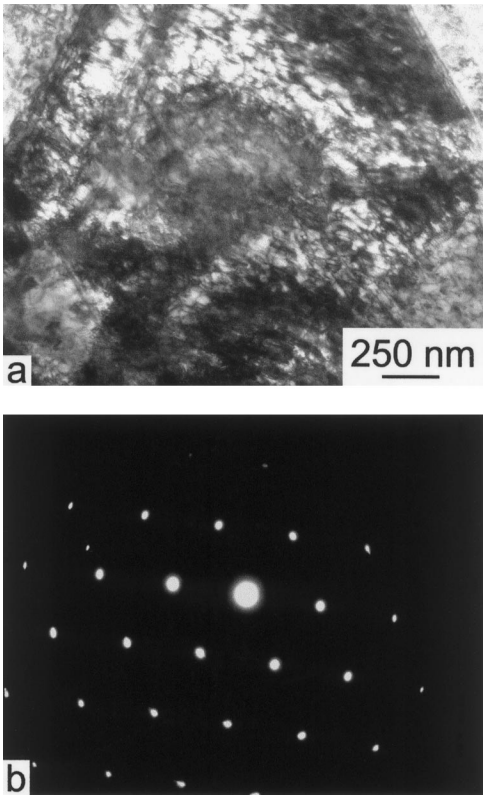

Fig. 13—(*a*) Bright-field transmission electron micrograph obtained from within the plastic zone of a fatigue-crack growth in a superelastic austenite specimen at 37 °C. A large number of dislocations are observed to be present in the material, and the martensite phase appears to be absent. Indeed, the crystal structure is confirmed to be *B*2 (*i.e.*, superelastic austenite) in the selected-area diffraction pattern shown in (*b*) for the zone axis [111].

directly on the fatigue fracture surface.* In equiatomic NiTi, 50 pct of the total diffracted intensity comes from a surface layer with a depth between 1 and 4 μm, as the angle of incident X-ray radiation varies from 15 to 80 deg; 99 pct of the total intensity comes from a layer at a depth of 7 to 27 μm for the same range in incident angles. At $\Delta K = 12$ MPa$\sqrt{}$m, the maximum plastic zone size, r_y, based on a yield strength = 1058 MPa, is ~27 μm. Hence, for intermediate and large ΔK, 99 pct of the diffracted intensity will originate from within the plastic zone at all incident angles of radiation. Even at lower stress-intensity ranges, *e.g.*, $\Delta K = 5$ MPa$\sqrt{}$m and $r_y \sim 5$ μm, 50 pct of the diffracted intensity will originate from within the plastic zone. The resulting X-ray diffraction spectrum of a fatigue fracture surface from a sample cycled in plane strain at 37 °C is shown in Figure 14; it is clear that the phase is austenite. We thus conclude that material in the vicinity of a growing fatigue crack in superelastic Nitinol (in plane strain at 37 °C) does not transform.

*The following calculations were based on mass absorption coefficients for nickel and titanium listed in "Elements of X-ray Diffraction" by Cullity[27] and copper K_α radiation with a wavelength equal to 1.542 Å.

3. *Suppression of the transformation at the crack tip*

Plane-strain fatigue-crack growth specimens tested at 37 °C did not transform, whereas monotonically loaded uniaxial tensile specimens did show the presence of a stress-

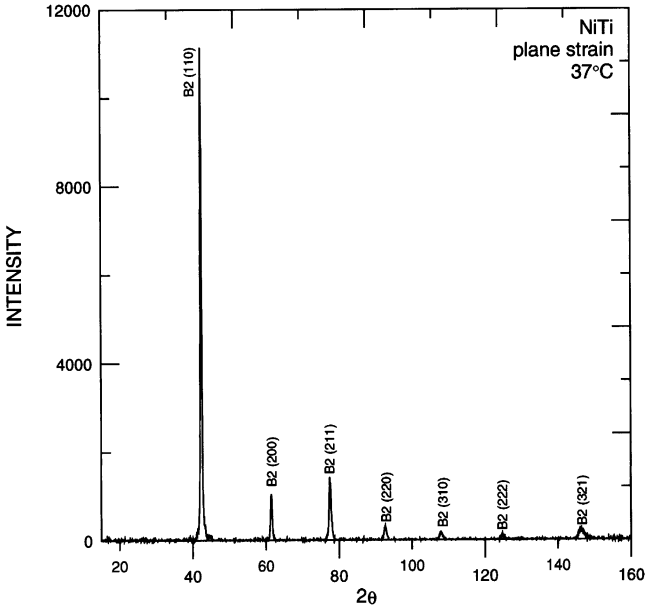

Fig. 14—X-ray diffraction spectrum obtained from the fatigue fracture surface of a (plane-strain) superelastic austenite DC(T) specimen tested at 37 °C. The data confirm that the crystal structure present in the crack wake after fatigue-crack propagation is *B*2, implying that the material *did not* transform to martensite along the crack flank.

induced martensitic transformation. One possible cause for this discrepancy is the triaxial stress conditions that exist at a crack tip, and in particular the presence of the large tensile hydrostatic stress state. Although the austenite-to-martensite transformation in Nitinol is dominated by shear, there does exist a small (less than ~0.5 pct) *negative* dilitational strain in the transformation from the *B2* to monoclinic structure.[3] The proposed argument here is that the *positive* hydrostatic stress state associated with the high degree of triaxiality of stresses ahead of the crack tip in *plane strain* would act to suppress the transformation; however, as discussed subsequently, this effect would be minimal under corresponding plane-stress conditions due to the absence of the stress triaxiality.

To examine the role of hydrostatic constraint and the triaxial stress state on the martensitic transformation, uniaxial tensile tests were performed under monotonic loading at 37 °C using unnotched and notched (0.75-mm root radius, 3.20-mm inner diameter) tensile bars. Since superelasticity exists in un-notched specimens, the question was whether the multiaxial stress state developed by constraint in the notched bars[28–31] could suppress the transformation.*

*Constraint can be quantified in terms of the ratio of the hydrostatic to equivalent stress, σ/σ_e. For uniaxial tension (in an un-notched sample), $\sigma/\sigma_c = 0.3$; for the notched tensile specimen used here,[32] $\sigma/\sigma_c = 1.1$; and for plane-strain conditions ahead of a crack tip, $\sigma/\sigma_c \sim 2$.[33]

Figure 15(a) is a plot of tensile data for superelastic austenite showing the change in diametral strain, ε_d, as a function of applied tensile axial strain in the un-notched sample. Two regions of constant ε_d with increasing axial strain are observed; these correspond to the stress-induced transformations of the R phase followed by the monoclinic martensite. The corresponding diametral strain data from the notched sample (Figure 15(b)), however, show no such plateaus, which indicate stress-induced transformations; instead, the

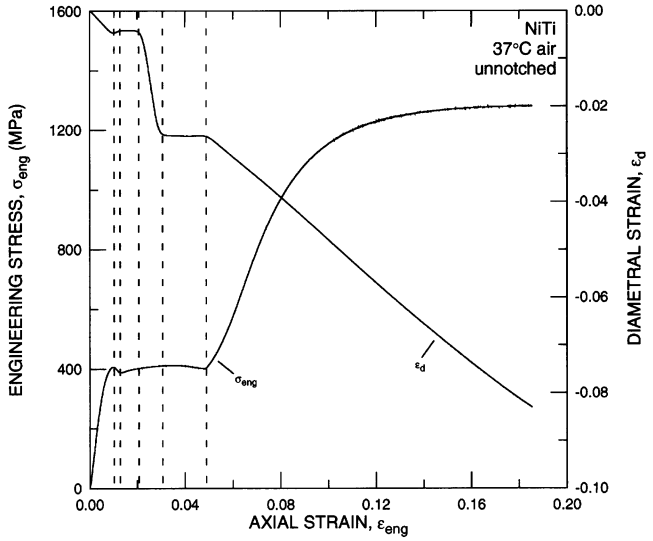

(*a*)

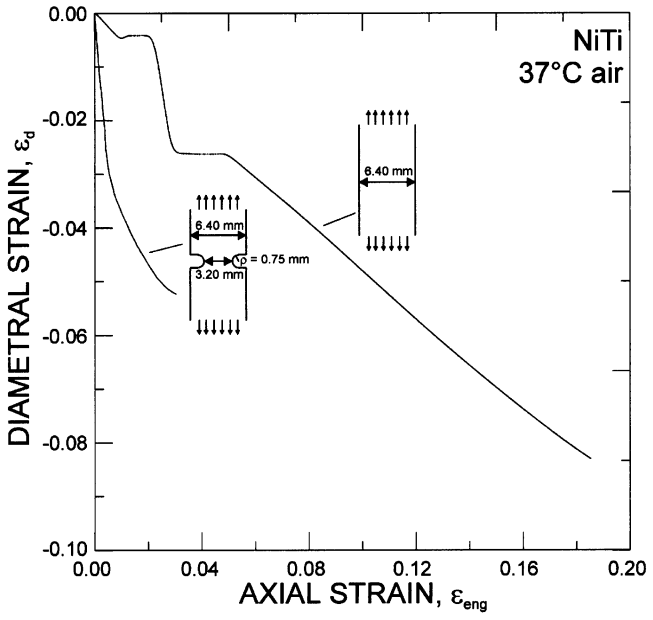

(*b*)

Fig. 15—Change in diametral strain, ε_d, as a function of tensile axial strain, ε_{eng}, in superelastic austenite at 37 °C (*a*) in un-notched samples (showing superimposed stress/strain curve and (*b*) in notched *vs* un-notched samples. Note the two plateaus in ε_d in (a), associated with stress-induced transformations to the R phase and monoclinic martensite, which are absent in the notched samples in (b).

data show linear behavior followed by a nonlinear region after the axial strain is greater than 0.5 pct. This result again implies that the transformation can be suppressed by a hydrostatic stress state, as no regions of constant diametral strain are observed.

4. *Plane strain* vs *plane stress*

We have shown so far that triaxial constraint can significantly affect superelasticity in Nitinol, such that the austenite-to-martensite transformation can be suppressed at the tip of a growing fatigue crack. However, the fatigue experiments at 37 °C were performed with samples that were thick enough

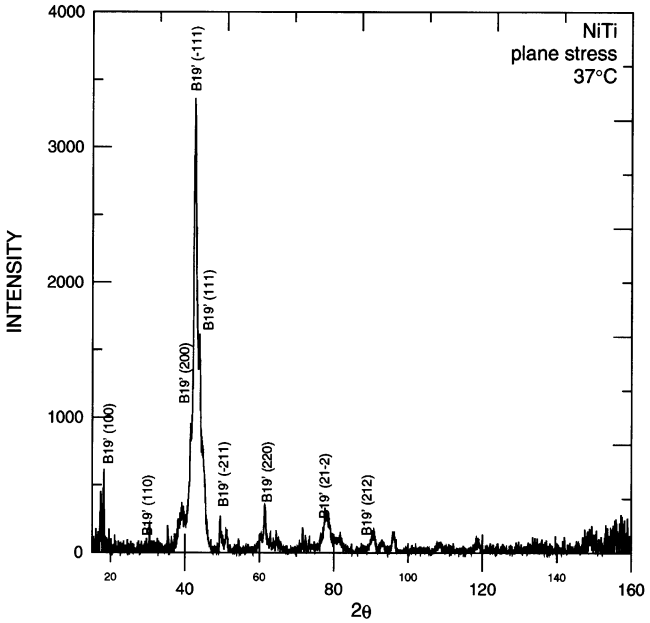

Fig. 16—X-ray spectrum obtained from the fatigue fracture surface of a plane-stress superelastic austenite DC(T) specimen tested at 37 °C. The data reveal that the material has transformed to the *B*19′ crystal structure, implying that the material *did* transform to martensite along the crack flank. Note, the planes are labeled according to the convention where **b** = 4.1205 Å is the unique axis (**a** = 4.6225 Å and **c** = 2.8854 Å) and $\beta = 96.81$ deg.

to be under plane-strain conditions.* This implies that in thin samples, wherein the limit of plane-stress conditions such triaxiality is not realized, the martensitic transformation should still occur *in situ* ahead of the crack tip, such that plasticity stabilized martensite should be detectable on the fatigue fracture surface. To investigate this effect, very thin DC(T) specimens ($B \sim 420$ μm) of superelastic NiTi were cycled at 37 °C at $R = 0.1$ (10 Hz) and the fatigue fracture surfaces examined using X-ray diffraction. Although the growth-rate data in these thin specimens were subject to significant scatter (Reference 26 provides details), the X-ray spectrum for crack growth at $\Delta K > 7$ MPa$\sqrt{\text{m}}$ (Figure 16) clearly reveals that under these unconstrained, nominally plane-stress conditions, transformation to martensite does occur.

*Plane-strain conditions can be considered to be prevalent when the out-of-plane thickness of the test specimen, *B*, is more than 13 to 15 times larger than the plastic-zone size. In terms of ASTM standard E-399, this occurs where $B > 2.5\,(K/\sigma_y)^2$, where K is the stress intensity and σ_y is the (plastic) yield stress.

IV. CONCLUDING REMARKS

Given the many applications that currently utilize Nitinol, including actuators, connectors, and smart antennas, and its rapidly expanding application into the biotechnology industries for endovascular stents, catheter guide wires, dental braces, *etc.*, the lack of published information on its resistance to cyclic fatigue, which represents a prime mechanism of failure, is alarming. The current study has shown that the characteristics of such fatigue-crack propagation behavior in NiTi are quite complex. Not only do the ΔK_{TH} thresholds and corresponding near-threshold growth rates ($\Delta K < 10$ MPa/m), which invariably govern the component lifetime, vary considerably with microstructure and temperature, but the occurrence of the superelastic transformation is found to be dependent on the prevailing hydrostatic stress state and degree of triaxiality. In unconstrained conditions, such as in uniaxial tension or ahead of a growing crack in (nominal) plane stress, the stress-induced transformation can occur quite readily, whereas in highly constrained conditions, such as ahead of a growing crack in plane strain, it appears to be suppressed. Moreover, the reversibility of the transformation is found to be severely affected by plastic strain.

Since superelastic austenite is the most commonly used microstructural condition for Nitinol in most biomedical applications, it is apparent that damage-tolerant design based on superelastic constitutive behavior may well be inaccurate due to this effect of crack-tip constraint on the transformation. Moreover, as noted in a previous study,[34] despite showing a relative insensitivity to accelerated crack-growth behavior in simulated physiological environments, the fatigue-crack growth resistance of superelastic Nitinol is one of the lowest of all metallic materials. Indeed, compared to other commonly used biomedical metallic alloys, such as titanium and Ti-6Al-4V, austenitic stainless steel, and CoCr alloys, superelastic Nitinol has significantly faster near-threshold growth rates and a ΔK_{TH} threshold that is a factor of ~2 to 5 times lower.[34] Since many of the biotechnology applications involve implanted devices where incipient failures can cause severe complications for the patient, it would appear to be prudent to invest in further studies into the fatigue properties of Nitinol before further applications are contemplated.

V. CONCLUSIONS

Based on an experimental study on the effect of microstructure, temperature, and superelasticity on fatigue-crack propagation behavior in a 55Ni-45Ti (wt pct) Nitinol alloy between 120 °C and −196 °C the following conclusions can be made.

1. With changes in temperature, NiTi was found to display several unique microstructure/stress-strain constitutive relationships, namely, stable austenite at $T = 120$ °C, superelastic austenite at $T = 37$ °C, and martensite at $T = -65$ °C and −196 °C.
2. Fatigue-crack growth in NiTi was observed to be sensitive to microstructure and temperature. In the stable austenite structure at 120 °C, crack-growth behavior (characterized in terms of ΔK) was found to be a function of the load ratio, with the ΔK_{TH} fatigue threshold varying from ~2.5 MPa$\sqrt{\text{m}}$ at $R = 0.1$ to ~1.5 MPa$\sqrt{\text{m}}$ at $R = 0.7$; growth rates in the Paris regime (~10^{-9} to 10^{-6} m/cycle) increased by almost an order of magnitude over the same range of increasing R.
3. Similar trends were seen during fatigue-crack growth in superelastic austenite at 37 °C; growth rates in the Paris regime were increased by an order of magnitude and ΔK_{TH} threshold values decreased from ~2.1 to ~1.1, with an increase in load ratio from $R = 0.1$ to 0.7.
4. When the fatigue-crack growth data in stable and superelastic austenite were replotted in terms of the effective

stress-intensity range, ΔK_{eff}, which "subtracts out" the influence of crack closure, load-ratio-independent behavior was found at near-threshold levels (at $\Delta K_{eff} < 4$ MPa$\sqrt{m}$), but not at higher growth rates. No such normalization was found at any stress-intensity level if growth rates were alternatively characterized in terms of K_{max}. Mechanistically, this implies that the origin of the load ratio effect, which is maximized at near-threshold growth rates, is crack closure.

5. By fitting such data to a modified Paris power-law relationship, crack-growth behavior in both stable and superelastic austenite was found to be equally dependent on ΔK and K_{max}. Specifically, the exponents on ΔK and K_{max} were calculated to be, respectively, 1.7 and 1.7 in stable austenite and 1.2 and 2.0 in superelastic austenite.
6. For the martensitic structure, resistance to fatigue-crack growth was enhanced with a decrease in temperature; in particular, ΔK_{TH} thresholds were increased from ~3.0 MPa$\sqrt{m}$ at −65 °C to ~5.0 MPa$\sqrt{m}$ at −196 °C. This effect was rationalized in terms of a change in crack closure. Above $\Delta K \sim 6.5$ MPa$\sqrt{m}$, fatigue-crack growth rates were essentially the same at both temperatures.
7. By comparing the fatigue behavior of the various microstructures in Nitinol, the fatigue-crack growth resistance of the martensite was found to be superior to that of the stable austenite, particularly in the near-threshold regime. The lowest resistance, however, in the form of the highest near-threshold growth rates and lowest ΔK_{TH} thresholds, was seen in the superelastic austenite.
8. Despite their markedly different monotonic constitutive behavior, the fatigue-crack propagation behavior of stable and superelastic austenite was remarkably similar, except at low growth rates near the threshold (where the ΔK_{TH} thresholds still only differed by ~0.5 MPa$\sqrt{m}$). This implies that superelasticity does not enhance crack-growth resistance in NiTi.
9. The superelastic effect was found to be degraded by plasticity in the form of stabilizing the martensitic phase. Specifically, when the applied strain exceeds the plastic yield strain (~8.5 pct), the reversibility of the martensitic transformation on unloading is diminished from essentially 100 to 29 pct, with most of the recovery being associated with linear elasticity.
10. The similarity of fatigue-crack propagation behavior in stable and superelastic austenite was found to be related to the fact that the superelastic phase transformation was suppressed by the hydrostatic stress state developed in the triaxial field ahead of a growing fatigue crack in plane strain. In contrast, for very thin superelastic austenite samples, where the high degree of triaxiality was not developed due to the prevailing "plane-stress" conditions, the stress-induced martensitic phase transformation *was* found to occur in the vicinity of the crack tip. The inhibition of the superelastic transformation by the hydrostatic tensile stress state ahead of the fatigue crack in plane strain is believed to be due to the fact that the austenite-to-martensite transformation in Nitinol involves a negative volume change.

ACKNOWLEDGMENTS

This work was supported by a gift to the University of California from Nitinol Devices and Components, Inc. (Fremont, CA). Thanks are due to Drs. T. Duerig and A. Pelton, NDC, for supplying the material and for helpful discussions.

REFERENCES

1. K.N. Melton and O. Mercier: *Acta Metall.*, 1979, vol. 27, pp. 137-44.
2. S. Miyazaki, M. Suizu, K. Otsuka, and T. Takashima: *Shape Memory Materials*, Proc. MRS Int. Meeting on Advanced Materials, K. Otsuka and K. Shimizu, eds., Materials Research Society, Pittsburgh, PA, 1989, vol. 9, pp. 263-8.
3. R.H. Dauskardt, T.W. Duerig, and R.O. Ritchie: *Shape Memory Materials*, Proc. MRS Int. Meeting on Advanced Materials, K. Otsuka and K. Shimizu, eds., Materials Research Society, Pittsburgh, PA, 1989, vol. 9, pp. 243-49.
4. W. Elber: *Eng. Fract. Mech.*, 1970, vol. 2, pp. 37-45.
5. R.O. Ritchie and W. Yu: in *Small Fatigue Cracks*, R.O. Ritchie and J. Lankford eds., TMS-AIME, Warrendale, PA, 1986, pp. 167-89.
6. G.M. Michal: Ph.D. Thesis, Stanford University, Palo Alto, CA, 1979.
7. E. Goo and R. Sinclair: *Acta Metall.*, 1985, vol. 33, pp. 1717-23.
8. G.M. Michal and R. Sinclair: *Acta Cryst. B*, 1981, vol. 37, pp. 1803-07.
9. A.S. Savvinov, V.P. Sivokha, and V.N. Khachin: *Phys. Met.*, 1985, vol. 5, pp. 1107-18.
10. T. Saburi and C.M. Wayman: *Acta Metall.*, 1979, vol. 27, pp. 979-95.
11. J.Y. Hwang and C.F. Yang: *Smart Materials Fabrication and Materials for Micro-Electro-Mechanical Systems*, Materials Research Society, Symposia Proceedings, A.P. Jardine, G.C. Johnson, A. Crowson, and M. Allen, eds., Materials Research Society, Pittsburgh, PA, 1992, vol. 276, pp. 183-88.
12. A.L. McKelvey and R.O. Ritchie: *Phil. Mag. A*, 2000, vol. 80, pp. 1759-68.
13. C.M. Wayman and T.W. Duerig: in *Engineering Aspects of Shape Memory Alloys*, T.W. Duerig, K.N. Melton, D. Stockel, and C.M. Wayman, eds., Butterworth Heinemann, London, 1990, pp. 3-17.
14. T.W. Duerig and R. Zadno: in *Engineering Aspects of Shape Memory Alloys*, T.W. Duerig, K.N. Melton, D. Stockel, and C.M. Wayman, eds., Butterworth Heinemann, London, 1990, pp. 369-83.
15. R.A. Schmidt and P.C. Paris: *Progress in Flaw Growth and Fracture Testing*, ASTM STP 536, ASTM, Philadelphia, PA, 1973, pp. 79-94.
16. R.O. Ritchie and J.F. Knott: *Acta Metall.*, 1973, vol. 21, pp. 639-48.
17. C.J. Gilbert, R.H. Dauskardt, and R.O. Ritchie: *J. Am. Ceram. Soc.*, 1995, vol. 78, pp. 2291-2300.
18. R.H. Dauskardt, M.R. James, J.R. Porter, and R.O. Ritchie: *J. Am. Ceram. Soc.*, 1992, vol. 75, pp. 759-71.
19. R.O. Ritchie: *Int. J. Fract.*, 1999, vol. 100, pp. 55-83.
20. J.P. Campbell, K.T. Venkateswara Rao, and R.O. Ritchie: *Metall. Mater. Trans. A*, 1999, vol. 30A, pp. 563-77.
21. K. Badrinarayanan, A.L. McKelvey, K.T. Venkateswara Rao, and R.O. Ritchie: *Metall. Mater. Trans. A*, 1996, vol. 27A, pp. 3781-92.
22. R.O. Ritchie: *Mater. Sci. Eng. A*, 1988, vol. 103, pp. 15-28.
23. Z. Mei and J.W. Morris Jr.: *Metall. Trans. A*, 1990, vol. 21A, pp. 3137-52.
24. S. Suresh: *Fatigue of Materials*, Cambridge University Press, New York, NY, 1991, p. 586.
25. E. Tschegg and S. Stanzl: *Acta Metall.*, 1981, vol. 29, pp. 33-40.
26. A.L. McKelvey: Ph.D. Thesis, University of California, Berkeley, CA, 1999.
27. B.D. Cullity: *Elements of X-ray Diffraction*, 2nd ed., Addison-Wesley Publishing Company, Inc., Reading, MA, 1978.
28. D.P. Clausing: *J. Mater.*, 1969, vol. 4, pp. 566-82.
29. D.P. Clausing: *Int. J. Fract. Mech.*, 1970, vol. 6, pp. 71-85.
30. J.W. Hancock and A.C. Mackenzie: *J. Mech. Phys. Solids*, 1976, vol. 24, pp. 147-69.
31. A.C. Mackenzie, J.W. Hancock, and D.K. Brown: *Eng. Fract. Mech.*, 1977, vol. 9, pp. 167-88.
32. P.W. Bridgeman: *Studies in Large Flow and Fracture*, McGraw-Hill, New York, NY, 1952.
33. J.R. Rice and M.A. Johnson: in *Inelastic Behavior of Solids*, M.F. Kanninen, ed., McGraw-Hill, New York, NY, 1970, pp. 641-72.
34. A.L. McKelvey and R.O. Ritchie: *J. Biomed. Mater. Res.*, 1999, vol. 47, pp. 301-08.